Analysis of Surface Temperature Accuracy in ASTER Images according to Land-Use Type

Bonggeun Song[1], Kyunghun Park[2]

[1] *Bureau of Ecological Conservation Research, National Institute of Ecology, 1210, Geumgang-ro, Maseo-myeon, Seocheon-gun, South Korea, bgsong@nie.re.kr*

2 Dept. of Environmental Engineering, Changwon National University, 20 Changwondaehak-ro, Uichang-gu, Changwon-si, Gyeongsangnam-do, South Korea, landpkh@changwon.ac.kr

dated : 15 May 2015

1. Introduction

Recently, surface temperature data derived from thermal infrared satellite imagery have been used in UHI (Urban heat island) studies. Satellite imagers in equipped with thermal infrared sensors are MODIS (Moderate resolution imaging spectra radiometer), Landsat TM/ETM+, and ASTER (Advanced space borne thermal emission and reflection radiometer). They have low spatial resolution, so understanding accurate feature of surface temperature in urban area is limited.

Various preceding studies have analyzing accuracy of surface temperature derived from thermal infrared satellite imagery with in-situ measurement (Hartz et al., 2006; Rigo et al., 2006; Yu and Hien, 2006; Lagios et al., 2007). However, studies about accuracy of surface temperature in accordance with land cover and land use are needed, because urban area has complex and diverse spatial characteristics.

Therefore, this study analyzed the accuracy of the surface temperature according to land use type in a thermal infrared satellite imagery (ASTER) in Changwon city, South Korea, and derived a calibration model for each land use type.

2. Methodology

2.1 Study site

Eight land use types such as Changwon National University (CNU) campus, urban park of 2 types, low-rise apartment, commercial facility, single residential, high-rise apartment, lawn square were selected from the urban areas of Changwon city (35°14'01.02"N, 128°41'19.95"E) (Figure 1). In CNU (1), buildings of about 10m height are arrayed widely apart. Urban parks (2, 3) are mainly composed of trees and lawn. Low-rise apartment (4) is covered with asphalts, and situated buildings of 5 floors. Site 5 is commercial facility; the buildings are mostly 40-50m in height, and land cover is covered with asphalt and concrete. Land cover in Single residential (6) is fabrics like site 5. Building height is approximately 5m. Land use type of Site 7 is high-rise apartment. There is composed of various land cover types such as trees, lawn, asphalts, sidewalk brick, and so on. Site 8 is lawn square covered by homogeneous land cover types.

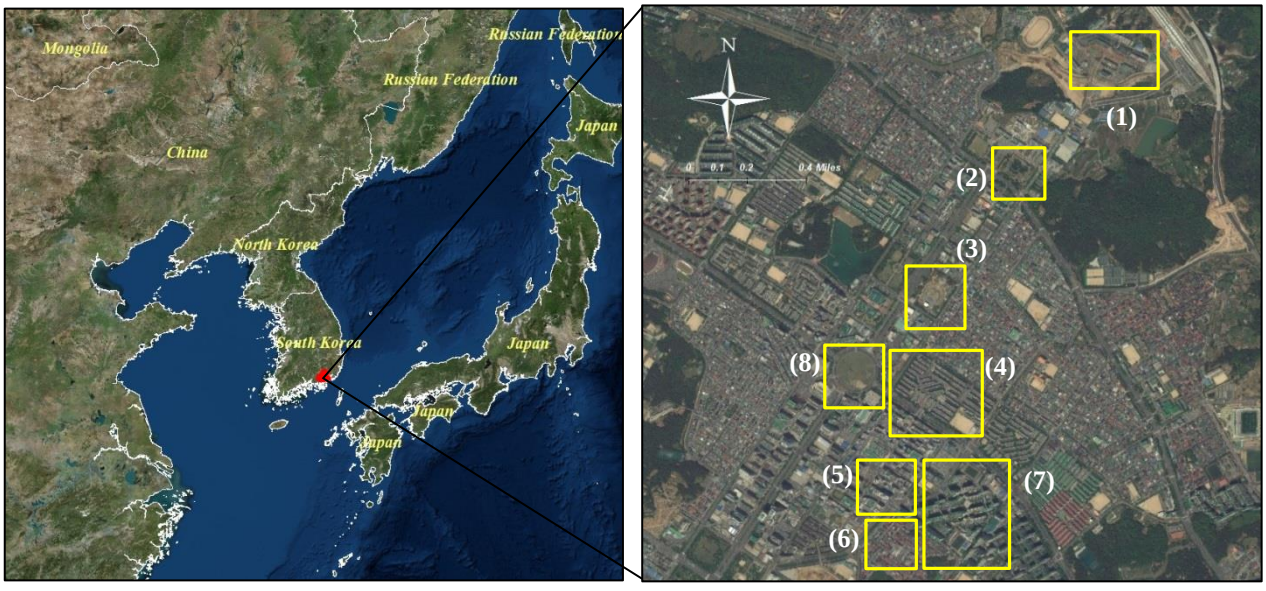

Figure 1. Study sites. (1) Changwon National University (CNU) campus, (2) Urban park 1, (3) Urban park 2, (4) Low-rise apartment, (5) Commercial facility, (6) Single residential, (7) High-rise apartment, (8) Lawn square

2.2 Collection of satellite imagery data

Thermal infrared imagery data were collected on 5 daytime and 3 nighttime of ASTER 2B03 product taken from June 2012 to August 2014. ASTER 2B03 product is generated at 8.15-11.65 μm (Kato and Yamaguchi, 2007). The spatial resolution is 90m, and it is pre-generated by the emissivity product ASTER 2B04 and the Temperature-Emissivity Separation (TES) algorithm (Gillespie et al., 1999; Hartz et al., 2006). The collected imagery data went through geometric correction and coordinate transformation with the Geodetic Reference System (GRS) 80 by application of the image-processing program PG-STEAMER ver. 4.2 (Pixoneer Corporation in South Korea)..

Table 1. ASTER satellite imagery collected during period of this study

Time	Date	Local time (UTC+9)
Daytime	07/28/2012	02:10 p.m.
	09/23/2012	02:16 p.m.
	06/29/2013	02:21 p.m.
	08/09/2013	02:20 p.m.
	08/12/2014	02:22 p.m.
Nighttime	09/21/2012	01:31 a.m.
	09/28/2012	01:37 a.m.
	08/14/2013	01:33 a.m.

2.3 Land cover data

Land cover data was constructed with land cover map from Changwon Environmental Atlas at a 1:1,1000 scale, site survey, and aerial photographs (spatial resolution: 10cm), classified to 21 types. During daytime, shaded areas are created by buildings and trees. So, shaded areas were included in land cover data through Hillshade analysis of the ArcGIS program.

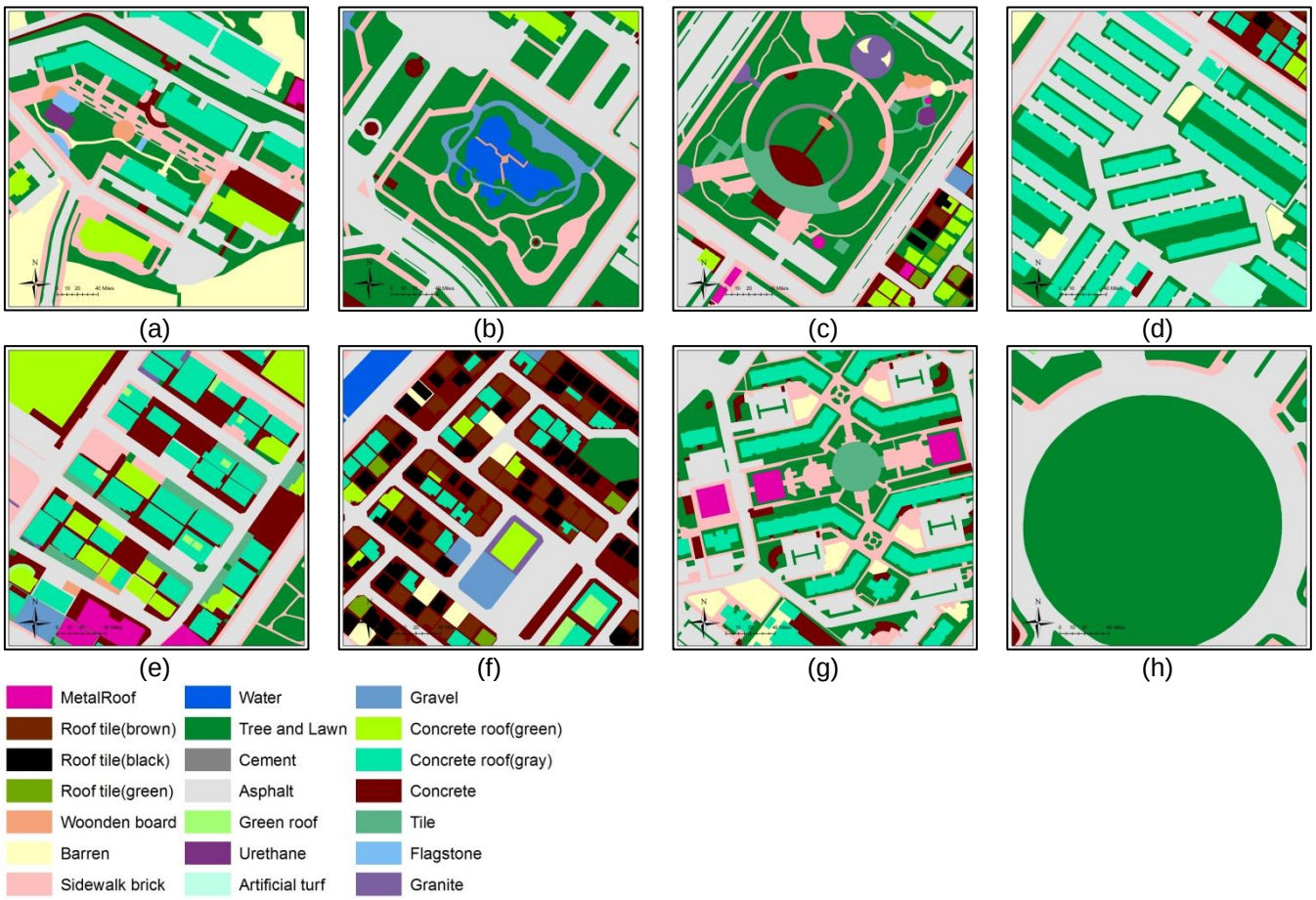

Figure 2. Land cover data of each study sites. (a) Changwon National University, (b) Urban park1, (c) Urban park2, (d) Low-rise apartment, (e) Commercial facility, (f) Single residential, (g) High-rise apartment, (h) Lawn square

2.4 Field measurement

2.4.1 Surface temperature

Measurement of surface temperature was carried out similar time with scanning of ASTER satellite imagery. Measurement point is total 628 points: Changwon national university 106 points, Urban park 1 88 points, Urban park 2 92 points, Low-rise apartment 86 points, Commercial facility 102 points, Single residential 66 points, High-rise apartment 82 points, Lawn square 6 points. Measurement time was 1 hour during scanning time of satellite imagery, 14:00 – 15:00 p.m. for daytime and 01:00 – 02:00 a.m. for nighttime. Surface temperature was measured at elevation of 10cm above the surface in the vertical direction with a thermal infrared thermometer (Testo 391, accuracy: ±1.5°C, emissivity: 0.95)

2.4.2 Emissivity

Regarding the measurement points, 190 points were selected in total according to the land cover type. In the study by Song and Park (2014), measurements were made for 3 day on May 27, June 5, and June 24, and this study added data measured on July 0 and July 11 of 2013, Measurements were made at 10:00 – 16:00.

Emissivity was calculated by application of the Stefan-Boltzmann equation shown in Formula (1), and terrestrial radiation and surface temperature, variables of the formula, were measured for each type of land cover and substituted into the formula as follows.

$$\varepsilon_i = \frac{L_i}{\sigma \times \varepsilon_{0.95} \times (273.15 + T_{si})^4} \quad (1)$$

Here, εi refers to the emissivity of the i material and Li indicates the terrestrial radiation of the i material (Wm-2). In addition, σ indicates the Stefan–Boltzmann constant 5.67 × 10-8 Wm-2K-4, ε0.95 indicates an emissivity of 0.95, and Tsi indicates the surface temperature (°C) of the i material.

2.5 Comparison of surface temperature between field measurement and satellite imagery

Figure 3 shows the method used for comparing ASTER surface temperatures with field measurement. Surface temperature of field measurement was calculated within a vector GRID of 90m×90m that was identical to the spatial resolution of the ASTER imagery. Average surface temperature based on field measurements was calculated by substituting the area ratio of each land cover type within the vector GRID and surface temperature data by land cover type measured in the field into Formula (2).

$$T_s = \sum_{i=1}^{n} \left[\left\{ \sqrt[4]{\frac{0.95}{\varepsilon_i}(273.15 + T_{si})^4} - 273.15 \right\} \times A_i \right] \quad (2)$$

Here, ε_i refers to emissivity of the i material, T_{si} indicates the surface temperature of the i material, and A_i indicates the area ratio of the i material.

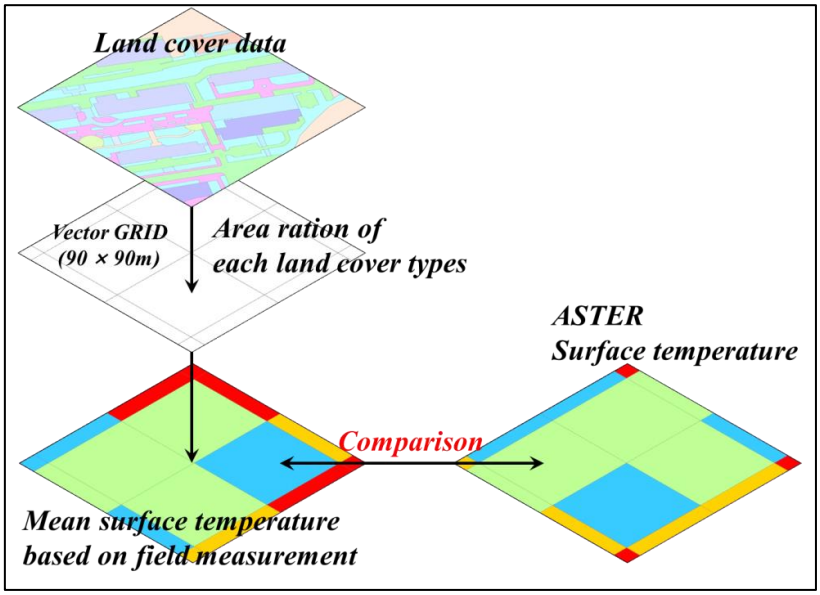

Figure 3. Method of comparing ASTER surface temperature imagery with field measured average surface temperature

3. Results and Discussion

3.1 ASTER surface temperature

The highest temperature during daytime was between 55°C and 60°C of June an August and the temperature decreased slightly to 47.7°C in September when autumn was approaching. The forest parks with greenery areas were lower than urban areas approximately 20°C. In nighttime, Difference between the highest and lowest surface temperature was about 10°C (Figure 4).

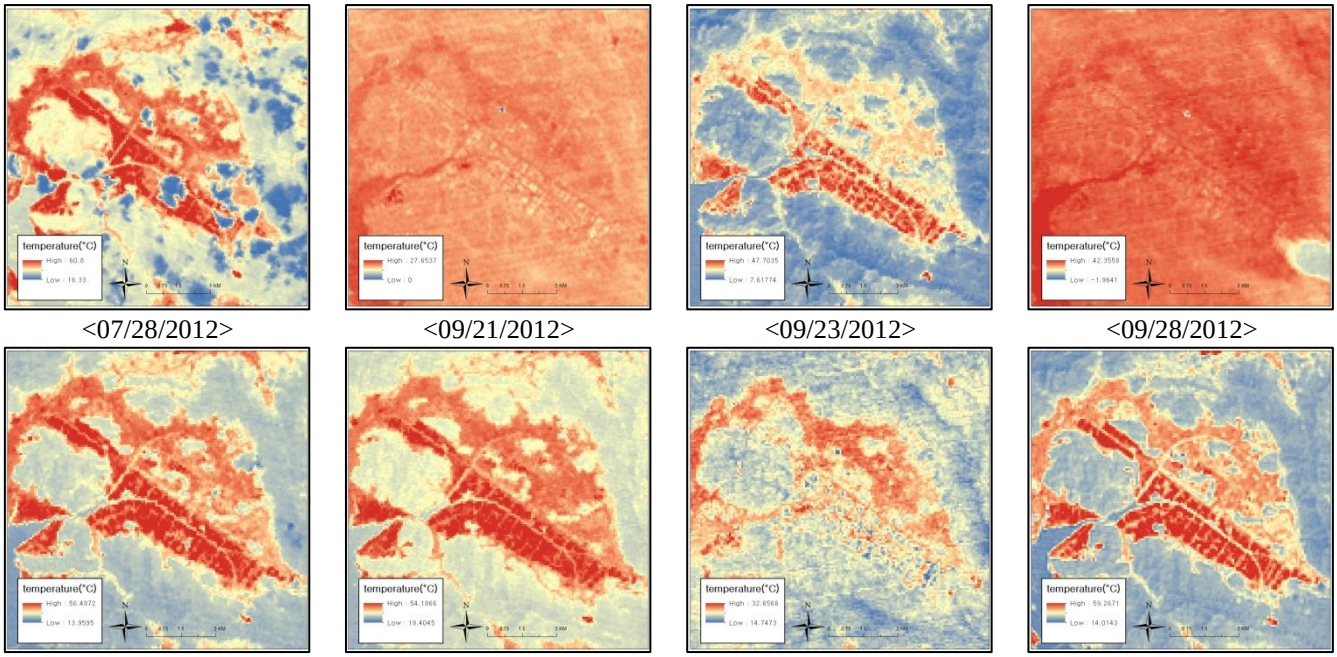

Figure 4. Surface temperature derived from ASTER satellite imagery collected from 2012 to 2014.

3.2 Field measurement

3.2.1 Emissivity

Land cover materials with the highest emissivity were black and green roof tiles measured at 1.000 and 0.990, respectively. Artificial land cover types such as cement (0.959), asphalt (0.972), urethane (0.987), artificial turf (0.979), and rooftop waterproof concrete (0.980) showed a tendency toward high emissivity values. In contrast, natural land cover types such as water (0.884), green roofs (0.930), and lawns (0.930) were associated with low recorded emissivity values.

Table 2. Emissivity of each land cover types

Land cover	N	Mean	Max.	Min.	S.D.	Land cover	N	Mean	Max.	Min.	S.D.
Metal roof	1	0.980	-	-	-	Green roof	1	0.93	-	-	-
Roof tile (brown)	2	0.990	1	0.980	0.014	Urethane	7	0.987	0.999	0.962	0.013
Roof tile (black)	1	1.000	-	-	-	Artificial turf	3	0.979	0.998	0.955	0.022
Roof tile (green)	1	0.990	-	-	-	Gravel	8	0.955	0.985	0.926	0.018
Wooden deck	7	0.944	0.997	0.802	0.067	Lawn	18	0.93	0.983	0.89	0.03
Sand and bare	11	0.942	0.987	0.814	0.05	Concrete	11	0.925	0.967	0.774	0.062
Sidewalk brick	44	0.962	0.999	0.839	0.025	Concrete roof (green)	1	0.98	-	-	-
Water	1	0.884	-	-	-	Concrete roof (gray)	1	0.98	-	-	-
Trees	5	0.946	0.971	0.923	0.02	Tile	11	0.951	0.986	0.87	0.036
Cement	16	0.959	0.987	0.928	0.015	Flagstone	7	0.969	0.987	0.953	0.012
Asphalt	20	0.972	0.998	0.931	0.016	Granite	13	0.956	0.998	0.865	0.034

3.2.2 Surface temperature of each land cover types

Land cover materials recording the highest surface temperatures during daytime were wooden decks (07/28/2012: 69.0°C, 09/23/2012: 52.2°C, 06/29/2013: 62.0°C, 08/09/2013: 62.9°C, 08/12/2014: 64.8°C), followed by urethane (07/28/2012: 66.2°C, 09/23/2012: 49.3°C, 06/29/2013: 54.0°C, 08/09/2013: 57.8°C). In general, artificial cover materials such as asphalt, cement, artificial turf, and concrete registered high temperatures. Conversely, natural materials such as water, trees, lawn, and green roofs recorded temperatures less than 40°C, which was approximately 20°C lower on average than the temperatures of artificial cover materials.

During nighttime, surface temperatures did not vary significantly, depending on the land cover type, compared with daytime. However, artificial materials such as cement (09/21/2012: 20.4°C, 09/28/2012: 19.0°C, 08/14/2013: 30.9°C), asphalt (09/21/2012: 19.6°C, 09/28/2012: 18.7°C, 08/14/2013: 31.2°C), concrete (09/21/2012: 19.7°C, 09/28/2012: 18.8°C, 08/14/2013: 30.1°C), and granite (09/21/2012: 21.4°C, 09/28/2012: 19.3°C, 08/14/2013: 29.4°C) were associated with high temperatures similar to daytime.

Land covert	Daytime					Nighttime		
	07/28/2012	09/23/2012	06/29/2013	08/09/2013	08/12/2014	09/21/2012	09/28/2012	08/14/2013
Metal roof	44.5	36.8	48	50	52.1	19.1	17	26
Roof tile (brown)	55.9	47.7	37.5	55.8	35.9	15.6	13.6	26.7
Roof tile (black)	57.4	46.9	36.6	56.4	36.9	15.6	15	27.2
Roof tile (green)	51.7	41.5	35.8	53.5	35.8	17.9	16.9	27.2
Wooden deck	69	52.2	62	62.9	64.8	12.1	12.2	24.1
Sand and Bare	47.8	30.6	43.6	48	34.3	15.7	15.1	26.7
Sidewalk brick	50.1	39.3	47.1	50.9	47.9	17.8	17.9	30
Water	27	21.4	25.1	31	26	17.3	19.9	26.9
Trees	36.3	25.6	28.4	36.8	30.1	15	16	26
Cement	55.9	50.3	48.8	53.3	51	20.4	19	30.9
Asphalt	58.5	45.5	53.1	57.2	54.5	19.6	18.7	31.2
Green roof	40	26.2	31.3	42	31	15.9	16.7	26.5
Urethane	66.2	49.3	54	57.8	54.2	15.3	14.4	31.1
Artificial turf	56.1	39.9	57.6	58.3	5.7	17	16.8	28.3
Gravel	52.3	37.5	44.8	50.3	47.8	13.9	15	27.8
Lawn	39	31.2	36.8	41.5	47.8	13.4	14.6	25.1
Concrete	54.2	40.5	47.1	52.7	51.4	19.7	18.8	30.1
Concrete roof (green)	57.4	43	49.2	58.6	52.5	18.1	18	30.7
Concrete roof (gray)	58.7	43.7	50.2	55.5	47.3	19.9	18.4	30.8
Tile	48.7	30.5	44.4	50.6	51.4	19.6	17.7	30
Flagstone	57.2	42.1	50.4	55.2	39.5	15.7	17.7	28.1
Granite	48	41.3	44.7	47	43.9	21.4	19.3	29.4

3.3 Accuracy of ASTER surface temperature

Figure 5 shows the RMSE analysis results of surface temperature comparisons between ASTER imagery and filed measurements. The RMSE (daytime: 7.7°C, nighttime: 2.1°C) was higher during daytime than during nighttime, and among the daytime results, the RMSE was the highest on July 28, 2012 at 10.7°C, because there was a slight cloud effect in the ASTER imagery. Also, RMSE was higher in the commercial facility area (9.2°C), single-residence area (8.6°C), and high-rise apartment area (8.8°C) with high building densities than in other areas. Difference was small in urban parks (6.7°C, 6.1°C) and lawn squares (5.8°C) with low building densities. These results are supported by the relatively large difference in field-measurement values in built-up areas such as the commercial facility and high-rise apartment areas in this study. Furthermore, ASTER imagery can sometimes be different from actual surface temperatures, as the off-nadir angle of ASTER imagery is 22.5° and ASTER measures the surface of the walls of buildings instead of the Earth's surface in high-density areas located on the edge of the image. During daytime, field-measured surface temperatures were higher than those from ASTER imagery.

In nighttime, surface temperatures measured in situ were lower than ASTER imagery, except on the midsummer night of August 14, 2013. Data from the lawn square (09/21/2012: 3.7°C, 09/28/2012: 3.9°C, 08/14/2013: 0.8°C) and urban park 1 (09/21/2012: 2.3°C, 09/28/2012: 2.4°C, 08/14/2013: 2.1°C) were found to have higher RMSE values than the other sites because roads were located nearby with heavy traffic and artificial heat generated by vehicles in the field was not measured accurately. Furthermore, the RMSE was higher in the fall season on September 21 (2.2°C) and September 28, 2012 (2.7°C) than in midsummer on August 14, 2013 (1.3°C).

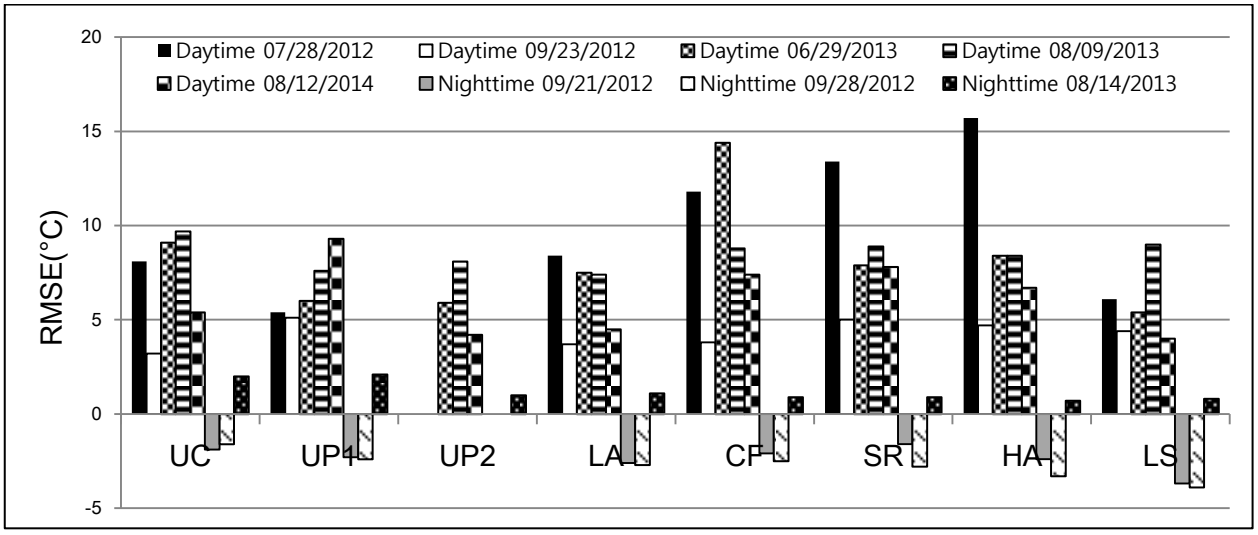

Figure 5. Root mean square error (RMSE) of the surface temperature between ASTER imagery and field measurements

4. Conclusion

The aim of this study is to develop a calibration model and analyze the accuracy of the Advanced Spaceborne Thermal Emission and Reflection Radiometer (ASTER) surface temperature data for each type of land use by utilizing field-measured surface temperature data targeting urban areas of Changwon City, South Korea. Analyses showed that the surface temperature measured in the field during the daytime was higher than that of satellite imageries by approximately 5°C to 10°C, and the gap was higher in built-up areas. The calibration models of surface temperature showed 60% explanatory power in areas other than urban parks, indicating that the models are reliable. During nighttime, except for the summer month of August, ASTER surface temperature was determined to be approximately 2°C higher in contrast to daytime. The calibration models of surface temperature registered very high explanatory power of more than 95%, however, the average surface temperature showed a significant difference depending on the timeframes. Therefore, the models must be complemented by considering more diverse timeframes. Therefore, there is a need to validate the accuracy and calibrate the models on the basis of field data to better utilize surface temperatures of satellite imagery. The results of this study are highly significant in this regard and will be useful in urban and environmental planning to resolve urban heat island effects.

Acknowledgment

This study was supported by the Basic Science Study Program through the National Study Foundation of Korea (NRF) via funding from the Ministry of Education, Science, and Technology (no. 2013-0095-0000).

References

Harlan, S.L., Brazel, A.J., Prashad, L., Stefanov, W.L., and Larsen, L., 2006, Neighborhood microclimates and vulnerability to heat stress. *Social Science and Medicine*, **63(11)**, 2847–2863.

Rigo, G., Parlow, E., and Oesch, D., 2006, Validation of satellite observed thermal emission with in-situ measurements over an urban surface. *Remote Sensing of Environment*, **104**, 201–210.

Yu, C. and Hien, W.N., 2006, Thermal benefits of city parks. *Energy and Buildings*, **38**, 105–120.

Lagios, E., Vassilopoulou, S., Sakkas, V., Dietrich, V., Damiata, B.N., & Ganas, A., 2007, Testing satellite and ground thermal imaging of low-temperature fumarolic field: The dormant Nisyros Volcano (Greece). *ISPRS Journal of Photogrammetry & Remote Sensing*, **62**, 447–460.

Kato, S. & Yamaguchi, Y., 2007, Estimation of storage heat flux in an urban area using ASTER data. *Remote Sensing of Environment*, **110**, 1–17.

Gillespie, A.R., Rokugawa, S., Hook, S.J., Matsunaga, T., & Kahle, A.B., 1999, Temperature/emissivity separation algorithm theoretical basis document, Version 2.4. Jet Propulsion Laboratory, Pasadena, March 22nd.

Hartz, D.A. Prashad, L., Hedquist, B.C., Golden, J., and Brazel, A.J., 2006, Linking satellite images and hand-held infrared thermography to observed neighborhood climate conditions. *Remote Sensing of Environment*, **104**, 190–200.

Song, B.G.and Park, K.H., 2014 Validation of ASTER surface temperature data with in situ measurements to evaluate heat islands in complex urban areas. Advances in Meteorology, Available online: http://dx.doi.org/10.1155/2014/620410.